surement of the rate of a ligand-based coupling reaction of a metal π-radical.

Oxidation and Reduction of CpCo(η^4-diolefins) (2 and 3). Although less intensively studied than the reduction of 1^+, the results on the η^4-diolefins generally are consistent with earlier observations about the redox pathways of CpCo(η^4-diolefin) compounds:

1. Cation radicals of the type $[CpCo(\eta^4\text{-diolefin})]^+$ are stable enough in dry CH_2Cl_2 to be observed by cyclic voltammetry and by ESR spectroscopy. Examples now include η^4-diolefin = cyclobutadienes[25] and the cyclodienes C_5H_6,[25] C_6H_8,[25] C_7H_{10} (present work), and C_8H_{12}.[8,25] Exceptions seem to involve η^4-diolefins that retain unsaturation because of unattached double bonds, such as cyclooctatetraene[8] and cycloheptatriene (present work). It is postulated that rapid rearrangement pathways exist for the latter π-ligands leading, at least initially, to isomerized metal π-complexes similar to those observed by Connelly et al. for $Fe(CO)_3$ analogues.[36]

2. Anion radicals of the type $[CpCo(\eta^4\text{-diolefin})]^-$ are also stable enough to be observed by cyclic voltammetry and, in some cases,[23] by ESR. Thus, an electron-transfer series involving d^7, d^8, and d^9 cobalt complexes exists:

$$[CpCo^{II}(\eta^4\text{-diolefin})]^+ \overset{e^-}{\rightleftharpoons} CpCo^{I}(\eta^4\text{-diolefin}) \overset{e^-}{\rightleftharpoons} [CpCo^{0}(\eta^4\text{-diolefin})]^-$$

E° values for the $d^7 \rightleftarrows d^8$ couple (Co^{II}/Co^{I}) show a smaller dependence on the nature of the diolefin (a range of +0.08 to +0.35 V is found) compared to the $d^8 \rightleftarrows d^9$ process (Co^{I}/Co^{0}) (range −1.8 to −2.6 V). Detailed ESR studies of the two series of ion radicals would be of interest to address the origin of this difference.

3. The favored reaction pathway for formally Co^0 π-anion radicals appears to be protonation of the polyolefin, followed by further reduction and protonation. The product is a more highly reduced polyolefin and implies an overall ECEC process:[23]

$$CpCo(\eta^4\text{-diolefin}) + 2e^- + 2H^+ \rightleftharpoons CpCo(\eta^4\text{-}H_2\text{diolefin})$$

This is only possible, of course, when the diolefin has unattached carbon–carbon double bonds (e.g., C_8H_8, C_8H_{10}, or C_7H_8) and is also found for $Fe(CO)_3$ analogues.[24] If all double bonds of the η^4-diolefin are already employed in coordination to the metal, as in C_8H_{12} or C_7H_{10}, E° for the Co^{I}/Co^{0} couple is very negative, and the ultimate fate of the anion radical is still unknown. The Co^0 anions usually undergo simple regeneration to the beginning Co^{I} complex by reaction with adventitious oxygen or other weak oxidizing agents.

Acknowledgment. This work was supported at the University of Vermont by the National Science Foundation (CHE83-03974) and at Zurich by the Swiss National Science Foundation (2.165-0.83).

Registry No. 1·PF_6, 78318-95-3; 2, 78318-94-2; 3, 70210-70-7; 4, 102210-37-7.

Supplementary Material Available: Complete listings of atomic coordinates, anisotropic thermal parameters, bond lengths and angles, hydrogen atom coordinates, and structure factor tables (22 pages). Ordering information is given on any current masthead page.

Structures and the Reversible Interconversion of Closo Rhodium–Triiron $M_4(\mu_4\text{-E})$ Clusters. Oxidation Reduction and ESR Spectra of Organometallic Anion and Cation Radicals

H. H. Ohst and J. K. Kochi*

Department of Chemistry, University of Houston, University Park, Houston, Texas 77004

Received November 19, 1985

The bicapped rhodium–triiron cluster $(C_5Me_5)RhFe_3(CO)_8(PPh)_2$ (I) is synthesized from the dianion of the triiron cluster $Fe_3(CO)_9(PPh)_2^{2-}$ and the dimeric rhodium complex $[(C_5Me_5)RhCl_2]_2$. The unsaturated cluster I reversibly binds CO to form the saturated cluster II. The interconversion I ⇌ II occurs with minimal alteration of the closo six-vertex framework which is characteristic of the bicapped tetranuclear clusters of the general formulation $M_4(\mu_4\text{-E})_2$, where E is a phosphinidene bridge. The unsaturated cluster undergoes a pair of one-electron reversible reductions to afford successively the anion $I^{-}\cdot$ and the dianion I^{2-}. Similarly the saturated cluster II undergoes a pair of one-electron reversible oxidations to afford successively the cation $II^{+}\cdot$ and the dication II^{2+}. These facile redox changes in the unsaturated and saturated clusters together with the ESR spectra of the ion radicals $I^{-}\cdot$ and $II^{+}\cdot$ confirm the theoretical predictions of Halet, Hoffmann, and Saillard for the bonding in closo six-vertex clusters. The rapid dissociative loss of CO in the anion radical of the saturated cluster ($II^{-}\cdot \rightarrow I^{-}\cdot + CO$) is also considered. The unsaturated cluster I ($RhFe_3P_2O_8C_{30}H_{25}$) crystallized in the monoclinic space group $P2_1/c$ with lattice constants a = 16.367 (3) Å, b = 10.684 (3) Å, c = 19.648 (5) Å, β = 110.37 (1)°, and Z = 4, and the saturated cluster II ($RhFe_3P_2O_9C_{31}H_{25}$) crystallized in the monoclinic space group $P2_1$ with lattice constants a = 9.260 (1) Å, b = 18.307 (3) Å, c = 19.562 (3) Å, β = 90.51 (1)°, and Z = 4.

Introduction

Active interest in transition-metal clusters continues in their syntheses, chemical reactions, catalytic properties, and novel structures.[1] Among these polynuclear systems, the capped organometallic clusters consisting of a planar array of four transition-metal atoms has attracted theoretical analysis. Thus following the discovery of the bicapped tetracobalt cluster $Co_4(CO)_{10}(\mu_4\text{-PPh})_2$ by Ryan and Dahl,[2] there has been developed various procedures for the

(1) Johnson, B. F. G., Ed. *Transition Metal Clusters*; Wiley: New York, 1980. Vahrenkamp, H. *Adv. Organomet. Chem.* **1983**, *22*, 169. Sappa, E.; Tiripicchio, A.; Braunstein, P. *Coord. Chem. Rev.* **1985**, *65*, 219.

(2) Ryan, R. C.; Dahl, L. F. *J. Am. Chem. Soc.* **1975**, *97*, 6904.

0276-7333/86/2305-1359$01.50/0

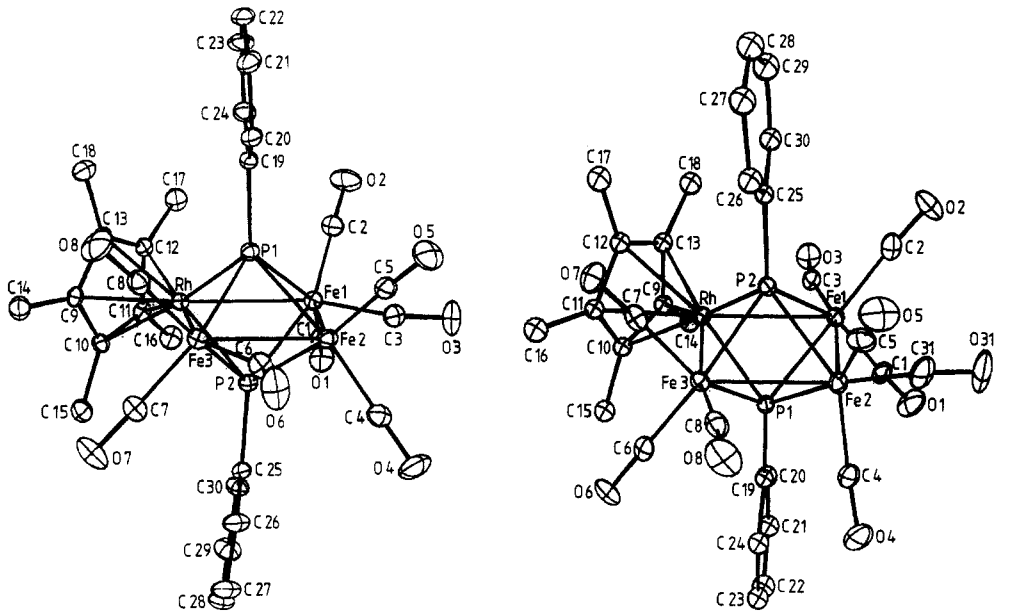

Figure 1. Ortep diagrams of the unsaturated cluster Cp′$RhFe_3(CO)_8(PPh)_2$ (I) (left) and the saturated cluster Cp′$RhFe_3(CO)_9(PPh)_2$ (II) (right) showing the similarity of the closo six-vertex framework and differences in the coordination at the Fe(2) center in the lower right. Hydrogens are omitted for clarity.

systematic synthesis,[3-5] studies of the chemical[6-11] and catalytic[12-14] properties, and theoretical insights into the structure and bonding[15] of related octahedral six-vertex organometallic clusters. Coordinative unsaturation in such clusters which are induced by the cleavage of either a metal–metal bond[10] or a metal–cap bond[16] and by the dissociative loss of coordinated ligands[17] are particularly pertinent to the development of their catalytic properties. In the latter regard, the observation by Vahrenkamp and Wolters[8] of the reversible binding of carbon monoxide to the tetrairon cluster $Fe_4(CO)_{11}(\mu_4\text{-PAr})_2$ is particularly noteworthy. Such an interconversion of an unsaturated cluster with a saturated one also offers an interesting opportunity to examine experimentally the recent theoretical analysis[15] of this family of square-bipyramidal $M_4(\mu_4\text{-E})_2$ clusters,[18] especially with regard to the applicability of the Wade–Mingos rules.[19,20]

Our preparation[16] of the bicapped triiron dianion $Fe_3(CO)_9(\mu_3\text{-PPh})_2^{2-}$ has enabled us to synthesize a six-vertex closo cluster I consisting of three iron and one rhodium

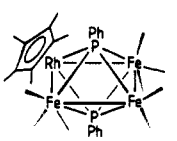

I.

atoms, which reversibly binds carbon monoxide. In this study, we describe how the examination of the redox properties of both the unsaturated and saturated analogues together with the ESR spectra of the corresponding anion radical and cation radical, respectively, provides experimental support for the electronic structure of this class of organometallic clusters presented by Halet, Hoffmann, and Saillard.[15]

Results

Synthesis and Structures of the Unsaturated and Saturated Rhodium–Triiron Clusters I and II. The bicapped triiron cluster $Fe_3(CO)_9(\mu_3\text{-PPh})_2$ undergoes a two-electron reduction to the dianion at a reversible potential of $E^0 = -1.30$ V vs. SCE in tetrahydrofuran (THF).[16] The red-brown dianion can also be prepared in THF by chemical reduction with sodium naphthalene according to the stoichiometry:

$$Fe_3(CO)_9(PPh)_2 + 2NaC_{10}H_8 \rightarrow Na_2[Fe_3(CO)_9(PPh)_2] + 2C_{10}H_8 \quad (1)$$

Utilizing the general strategy for cluster synthesis,[21] we find that the treatment of the carbonylmetalate dianion with the dimeric rhodium dihalide $[(C_5Me_2)RhCl_2]_2$ at −78 °C leads to the mixed-metal cluster I according to eq 2.

$$2Na_2[Fe_3(CO)_9(PPh)_2] + [(C_5Me_5)RhCl_2]_2 \rightarrow \underset{\text{I}}{2(C_5Me_5)RhFe_3(CO)_8(PPh)_2} + 4NaCl + 2CO \quad (2)$$

However only 20% of the triiron dianion was converted to I. The inspection of the ^{31}P NMR spectrum of the

(3) Vahrenkamp, H.; Wucherer, E. J. *Angew. Chem.* **1981**, *93*, 715.
(4) Vahrenkamp, H.; Wucherer, E. J.; Wolters, D. *Chem. Ber.* **1983**, *116*, 1219.
(5) Lang, H.; Zsolnai, L.; Huttner, G. *J. Organomet. Chem.* **1985**, *282*, 23.
(6) Ryan, R. C. Ph.D. Thesis, University of Wisconsin, Madison, WI, 1976.
(7) O'Connor, J. P. Ph.D. Thesis; University of Wisconsin, Madison, WI, 1977.
(8) Vahrenkamp, H.; Wolters, D. *Organometallics* **1982**, *1*, 874.
(9) Field, J. S.; Haynes, R. J.; Suit, D. N.; Natarajan, K.; Scheidsteger, O.; Huttner, G. *J. Organomet. Chem.* **1982**, *240*, C23.
(10) Richmond, M. G.; Korp, J. D.; Kochi, J. K. *J. Chem. Soc., Chem. Commun.* **1985**, *1*.
(11) Richmond, M. G.; Kochi, J. K. *Inorg. Chem.*, in press.
(12) Ryan, R. C.; Pittman, C. U., Jr.; O'Connor, J. P. *J. Am. Chem. Soc.* **1977**, *99*, 1986.
(13) Pittman, C. U., Jr.; Wilemon, G. M.; Wilson, W. D.; Ryan, R. C. *Angew. Chem.* **1980**, *92*, 494.
(14) Ryan, R. C.; Pittman, C. U., Jr.; O'Connor, J. P.; Dahl, L. F. *J. Organomet. Chem.* **1980**, *193*, 247.
(15) Halet, J.-F.; Hoffmann, R.; Saillard, J.-Y. *Inorg. Chem.* **1985**, *24*, 1695.
(16) Ohst H. H.; Kochi, J. K. *Inorg. Chem.*, in press.
(17) See, e.g.: (a) Muetterties, E. L.; Krause, M. J. *Angew. Chem., Int. Ed. Engl.* **1983**, *22*, 135. (b) Geoffroy, G. L. *Acc. Chem. Res.* **1980**, *13*, 469. (c) See also ref 1.
(18) M is usually a group VIII metal and tetracoordinate E is S, Te, PR, AsR, GeR, etc.
(19) Wade, K. *Adv. Inorg. Chem. Radiochem.* **1976**, *18*, 1. See also: Wade, K. In *In Transition Metal Clusters*; Johnson, B. F. G., Ed.; Wiley: New York, 1980; Chapter 3.
(20) Mingos, D. M. P. *Nature (London), Phys. Sci.* **1972**, *236*, 99.
(21) Gladfelter, W. L.; Geoffroy, G. C. *Adv. Organomet. Chem.* **1980**, *18*, 207.

Table I. Selected Bond Lengths (Å) and Angles (deg) in I and II

Bond Lengths

atoms		dist	
A	B	I	II
Rh	Fe(1)	2.769 (1)	2.762 (1)
Rh	Fe(3)	2.772 (1)	2.700 (1)
Fe(1)	Fe(2)	2.551 (1)	2.659 (1)
Fe(2)	Fe(3)	2.506 (1)	2.657 (1)
Rh	P(1)	2.270 (1)	2.264 (2)
Rh	P(2)	2.272 (1)	2.275 (2)
Fe(1)	P(1)	2.312 (1)	2.314 (2)
Fe(1)	P(2)	2.271 (1)	2.322 (2)
Fe(2)	P(1)	2.353 (1)	2.317 (2)
Fe(2)	P(2)	2.387 (1)	2.347 (2)
Fe(3)	P(1)	2.292 (1)	2.284 (2)
Fe(3)	P(2)	2.271 (1)	2.289 (2)
P(1)	P(2)	2.666 (1)	2.579

Bond Angles

atoms			angle	
A	B	C	I	II[a]
Fe(1)	Rh	Fe(3)	83.42 (1)	88.44 (3)
Rh	Fe(1)	Fe(2)	91.01 (1)	89.30 (3)
Fe(1)	Fe(2)	Fe(3)	93.61 (1)	91.56 (4)
Rh	Fe(3)	Fe(2)	91.91 (1)	90.70 (4)

[a] For one of the pair of independent molecules per unit cell.

reaction mixture indicated that most (80%) of it was oxidized by the rhodium(III) complex back to $Fe_3(CO)_9(PPh)_2$, which was removed by extraction with hexane following evaporation of the THF solvent in vacuo. The cluster I was isolated in 15% yield as black crystals by extraction of the residue with benzene.

The brown-black solution of the unsaturated cluster I in toluene was exposed to 1 atm of carbon monoxide. After 8 h, an aliquot of hexane was carefully added as a separate layer, which upon slow diffusion led to pure red-black crystals of II in 90% yield, i.e., eq 3. The reversibility of

$$\underset{\text{I}}{(C_5Me_5)RhFe_3(CO)_8(PPh)_2} + CO \rightleftharpoons \underset{\text{II}}{(C_5Me_5)RhFe_3(CO)_9(PPh)_2} \quad (3)$$

CO ligation in eq 3 is indicated by its slow reversion to I upon standing (in toluene solution). The unsaturated cluster could be recovered quantitatively by evacuating the solution.

The molecular structures of I and II were determined by X-ray crystallography.[16] The Ortep diagram of I is reproduced in Figure 1a to illustrate the presence of the formally unsaturated Fe(2) center, which is stabilized by a pair of semibridging carbonyl groups (∠Fe–C–O = 151° and 155°). The addition of 1 mol of CO leads to II in Figure 1b, showing the existence of only terminal carbonyl groups. The conversion of I to II is also accompanied by a slight elongation of the Fe–Fe bonds and a minor distortion in the $RhFe_3$ square plane.

For convenience, some of the relevant bond distances and angles in I and II are summarized in Table I. The comparison of these structural parameters shows that aside from some minor differences, the basic structure of the $RhFe_3P_2$ framework in the unsaturated cluster remains essentially unaltered upon its conversion to the saturated derivative.[22] Accordingly, we carried out comparative

(22) Such an interconversion is unusual, except for the earlier study of $Fe_4(CO)_{11}(PPh)_2$ by Vahrenkamp and Wolters.[8] For example, the addition of CO to the analogous unsaturated tetraruthenium cluster $Ru_4(CO)_{11}(\mu_4\text{-}PPh)_2$ leads to deep-seated cluster alteration by cleavages of a Ru–Ru bond and a pair of Ru–P bonds.[9]

Table II. The NMR Spectra of I and II[a]

nucleus	group	I	II
$^1H^b$	$C_5(CH_3)_5$	2.25 (t, $^4J_{PH}$ = 1.7 Hz)	1.78 (t, $^4J_{PH}$ = 1.5 Hz)
$^1H^b$	C_6H_5	6.6–7.3 (m)	7.4–8.0 (m)
$^{31}P^c$	P	227.6 (d, $^1J_{RhP}$ = 97 Hz)	319.6 (d, $^1J_{RhP}$ = 82 Hz)

[a] In $CDCl_3$ at 25 °C. [b] δ relative to interval Me_4Si. [c] δ relative to external 85% H_3PO_4.

studies of I and II relative to (a) the phosphinidene cap from NMR spectra, (b) the redox potentials by cyclic voltammetry, and (c) the ESR spectra of the anion radical and the cation radical, as presented individually below.

A. Comparison of the ^1H and ^{31}P NMR Spectra of I and II. The NMR spectra of the unsaturated cluster I and the saturated cluster II show similar nuclear hyperfine splitting patterns, but the chemical shifts are consistently displaced relative to each other. For example in the ^1H NMR spectrum, there is a significant difference in the chemical shifts of the aromatic protons, those in I being displaced ~0.6 ppm upfield relative to those in II (Table II). Similarly in the ^{31}P NMR spectra, the chemical shift of δ 228 for the phosphinidene caps in I corresponds to a displacement of roughly 100 ppm relative to those at δ 320 for the saturated cluster II. As a comparison for the latter, the closest available ^{31}P data is a chemical shift of δ 317 for the triiron cluster $Fe_3(CO)_9(\mu_3\text{-}PPh)_2$.[16] The upfield ^1H and ^{31}P shifts of the phenylphosphinidene bridges in I relative to those in II accords with Vahrenkamp's description of the ring current effects present in the M_4 core of the unsaturated cluster.[4,23] Furthermore, such a formulation is consistent with the downfield shift of the ^1H resonance for the peripheral methyl groups in the unsaturated cluster I relative to that in II (Table II). It also accords with the differences in the magnitudes of the observed couplings of the rhodium atom which splits the resonances of the phosphinidene caps into doublets in both I and II. Thus the value of $J_{P\text{-}Rh}$ = 97 Hz in I is significantly larger than the coupling of 82 Hz in the saturated cluster II in expectation with an increased interaction of the phosphinidene bridge in the more unsaturated core.[24]

B. Oxidation Reduction of the Rhodium–Triiron Clusters I and II. The redox behavior of the saturated and unsaturated clusters I and II were compared by cyclic voltammetry at a platinum electrode in tetrahydrofuran containing 0.3 M tetra-*n*-butylammonium perchlorate (TBAP).

The initial cathodic scan cyclic voltammogram of the unsaturated cluster I consists of two well-defined, reversible one-electron waves A and B at the negative potentials of $E_{1/2}$ –0.46 and –1.34 V vs. SCE, as shown in Figure 2,[26] i.e., eq 4. By contrast, the oxidation of I occurs by an

$$\underset{\text{I}}{Cp'RhFe_3(CO)_8(PPh)_2} \overset{[A]}{\rightleftharpoons} Cp'RhFe_3(CO)_8(PPh)_2^{-} \overset{[B]}{\rightleftharpoons} \underset{\text{I}^{2-}}{Cp'RhFe_3(CO)_8(PPh)_2^{2-}} \quad (4)$$

(23) Vahrenkamp, H.; Wolters, D. *J. Organomet. Chem.* **1982**, *224*, C17.

(24) The only available $^{31}P\{^1H\}$ NMR data for comparison are given for $Rh_4(\mu_4\text{-}PPh)_2(C_8H_{12})_4$: $\delta(^{31}P)$ + 65.8 (quintet, $^1J_{RhP}$ = 47.8 Hz).[25]

(25) Burkhardt, E. W.; Mercer, W. C.; Geoffroy, G. L.; Rheingold, A. L.; Fultz, W. C. *J. Chem. Soc., Chem. Commun.* **1983**, *1251*.

(26) Hereafter the reversible potentials are given as $E_{1/2} = {}^1/_2(E_p^a + E_p^c) \simeq E^0$, where E_p^a and E_p^c refer to the CV peak potentials of the anodic and cathodic waves, respectively.[27]

(27) Howell, J. O.; Goncalves, J. M.; Amatore, C.; Klasinc, L.; Wightman, R. M.; Kochi, J. K. *J. Am. Chem. Soc.* **1984**, *106*, 3968.

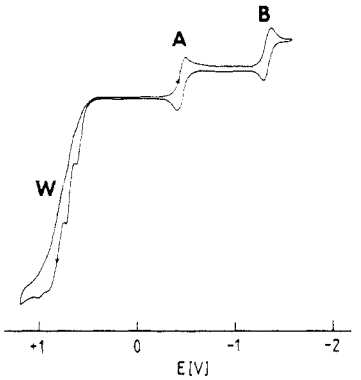

Figure 2. Initial cathodic scan cyclic voltammogram of the unsaturated cluster $Cp'RhFe_3(CO)_8(PPh)_2$ ($\sim 1 \times 10^{-3}$ M I) in THF containing 0.3 M TBAP at 10 mV s^{-1} and 25 °C which shows the reversible, one-electron reduction couples A and B to $I^{-}\cdot$ and I^{2-}, respectively, and the composite irreversible oxidation wave W.

Table III. Cyclic Voltammetric Parameters for I and II[a]

triiron cluster	wave	V, mV s^{-1}	E_p^c, V	E_p^a, V	$E_{1/2}$, V
I	A	10	0.50	−0.42	−0.46
I	B	10	−1.38	−1.30	−1.34
I	W_1	10		+0.61	
I	W_2	10		+0.71	
I	W_3	10		+0.89	
I	W_4	10		+1.02	
II	X	20	+0.39	+0.46	+0.42
		50	+0.40	+0.48	+0.44
		100	+0.40	+0.48	+0.44
		200	+0.39	+0.46	+0.43
II	Y	20		+0.99	
		50	+0.94	+1.02	+0.98
		100	+0.94	+1.01	+0.97
		200	+0.92	+1.00	+0.96
II	C	20	−0.48		
		50	−0.46		
		100	−0.46		
		200	−0.48		
II	D	20	−1.14		
		50	−1.11		
		100	−1.09		
		200	−1.12		
II	E	20	−1.37	−1.28	1.32
		50	−1.35	−1.26	−1.31
		100	−1.35	−1.27	−1.31
		200	−1.27	−1.36	−1.32
II	F	20		−0.42	
		50		−0.41	
		100		−0.41	
		200		−0.41	

[a] In THF containing 0.3 M TBAP at 25 °C.

irreversible multielectron process commencing at ~0.6 V (Table III). For example, at a CV scan rate of 10 mV s^{-1}, four distinct anodic waves W can be discerned at E_p = 0.61, 0.71, 0.89, and 1.02 V. At an increased scan rate of 500 mV s^{-1}, only two anodic waves W_1 and W_2 are resolved at E_p = 0.79 and 0.98 V, but they remain chemically irreversible even up to 20 V s^{-1}.

The initial anodic scan cyclic voltammogram of the saturated cluster II under an atmosphere of CO consists of two well-defined, reversible oxidation waves X and Y at the positive potentials of $E_{1/2}$ = 0.44 and 0.97 V, respectively, as shown in Figure 3 (see eq 5). The reductive

$$\underset{\text{II}}{CP'RhFe_3(CO)_9(PPh)_2} \overset{[X]}{\rightleftharpoons} \underset{\text{II}^{+}\cdot}{Cp'RhFe_3(CO)_9(PPh)_2^{+}} \overset{[Y]}{\rightleftharpoons} \underset{\text{II}^{2+}}{Cp'RhFe_3(CO)_9(PPh)^{2+}} \quad (5)$$

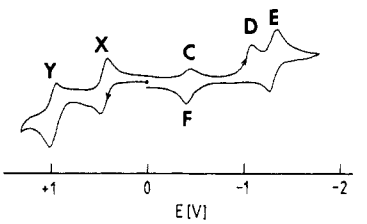

Figure 3. Initial anodic scan cyclic voltammogram of the saturated cluster $Cp'RhFe_3(CO)_9(PPh)_2$ ($\sim 1 \times 10^{-3}$ M II) in THF under a CO atmosphere and containing 0.3 M TBAP at 100 mV s^{-1} and 25 °C, which shows the reversible, one-electron oxidation couples X and Y to $II^{+}\cdot$ and II^{2+}, respectively, and the irreversible reduction wave D to $II^{-}\cdot$. For the CV waves C, E and F, see text.

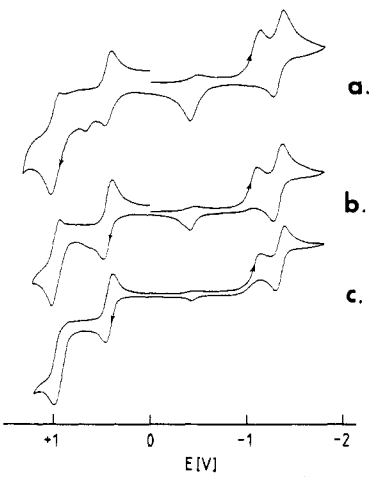

Figure 4. Initial negative scan cyclic voltammograms of the saturated cluster II ($\sim 1 \times 10^{-3}$ M) in THF containing 0.3 M TBAP at 25 °C and scan rates of (a) 200, (b) 50, and (c) 20 mV s^{-1}. Note the decrease in the peak current of the CV wave F and the resolution of X and Y.

behavior of II in Figure 3 is more complex and requires some elaboration. Thus three cathodic waves C, D, and E are observed at E_p^c = −0.46, −1.09, and −1.35 V, respectively. The last CV wave E is chemically reversible with $E_{1/2}$ = −1.32 V, which is identical with wave B of the unsaturated cluster I. Similarly the first CV wave C also appears to be reversible with $E_{1/2}$ = −0.46 which is the same as that for wave A of the unsaturated cluster in Figure 2. However, its peak current ratio $i_p^a/i_p^c > 1$ indicates that a component of the anodic wave F derives from an additional source. This can be attributed to the irreversible CV wave D, which we assign to the reduction of the saturated cluster II, i.e., eq 6, followed by the rapid

$$\underset{\text{II}}{Cp'RhFe_3(CO)_9(PPh)_2} + e \xrightarrow{[E_p^c = -1.11\ \text{V}]} \underset{\text{II}^{-}\cdot}{Cp'RhFe_3(CO)_9(PPh)_2^{-}\cdot} \quad (6)$$

dissociative loss of CO[28] to afford the anion radical $I^{-}\cdot$ of the unsaturated cluster in eq 7.

$$\underset{\text{II}^{-}\cdot}{Cp'RhFe_3(CO)_9(PPh)_2^{-}\cdot} \xrightarrow{\text{fast}} \underset{\text{I}^{-}\cdot}{Cp'RhFe_3(CO)_8(PPh)_2^{-}\cdot} + CO \quad (7)$$

The overall process for such an irreversible reduction is

(28) Compare: Darchen, A.; Mahe, C.; Patin, H. *Nouv. J. Chim.* **1982**, *6*, 539.
(29) Such a CV behavior attendant upon reduction of a metal carbonyl has been observed in mononuclear systems.[30]
(30) Narayanan, B. A.; Amatore, C.; Kochi, J. K. *J. Chem. Soc., Chem. Commun.* **1983**, 387.

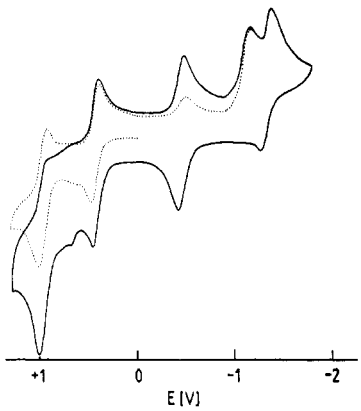

Figure 5. Cyclic voltammetric study of the oxidation of the saturated cluster II in THF under a CO atmosphere and containing 0.3 M TBAP at 25 °C: (---) initial anodic single sweep; (—) steady state at repetitive scans at 500 mV s^{-1}.

tantamount ot the formation of the reduced unsaturated cluster $I^{-}\cdot$ directly from the saturated cluster II, i.e., eq 8.

$$\underset{\text{II}}{Cp'RhFe_3(CO)_9(PPh)_2} + e \rightarrow \underset{\text{I}^{-}\cdot}{Cp'RhFe_3(CO)_8(PPh)_2^{-}\cdot} + CO \quad (8)$$

The initial negative scan cyclic voltammogram of the saturated cluster II in Figure 4 shows the same transient electrochemical behavior in the negative potential region as that observed in Figure 3. Minor amounts of I (as shown by the limited peak current of the CV wave C) are initially present as a result of the dissociative equilibrium in eq 3. The reductive behavior of the saturated cluster is dependent on the CV scan rate. Most noticeably, the peak current of the anodic wave F decreases with scan rate until it is barely perceptible at 20 mV s^{-1} in Figure 4c. We attribute this behavior to the reversibility of CO dissociation in eq 7 which effectively reduces the amount of $I^{-}\cdot$ during the time interval for the reverse scan, i.e., eq 9.

$$\underset{\text{I}^{-}\cdot}{Cp'RhFe_3(CO)_8(PPh)_2^{-}\cdot} + CO \rightarrow \underset{\text{II}^{-}\cdot}{Cp'Fe_3(CO)_9(PPh)_2^{-}\cdot} \quad (9)$$

This conclusion is supported by the CV behavior observed in the positive potential region of Figure 4, showing a superposition of the CV waves X and Y with W from Figures 3 and 2, respectively. This is particularly noticeable at a sweep rate of 200 mV s^{-1} in Figure 4a. Such a composite results from the simultaneous oxidation of II as well as I which is generated during the initial negative sweep, as in eq 8. At a slow sweep rate of 20 mV s^{-1} in Figure 4c, the unsaturated $I^{-}\cdot$ does not persist during the reverse scan owing to CO reversibility. As a result, this portion of the cyclic voltammogram closely resembles that in Figure 3. The same conclusion is reached by a comparison of the initial positive scan with the cyclic voltammogram obtained at steady state in Figure 5. The positive potential region of the steady state cyclic voltammogram is clearly a composite of the oxidation of the saturated and the unsaturated clusters.

The quenching of the unsaturated anion radical can also be effected by other ligands such as trimethyl phosphite, e.g., eq 10. Thus a cyclic voltammogram very similar to

$$Cp'RhFe_3(CO)_8(PPh)_2^{-}\cdot + P(OMe)_3 \rightarrow Cp'RhFe_3(CO)_8(PPh)_2[P(OMe)_3]^{-}\cdot \quad (10)$$

that observed in Figure 4c is obtained (for the negative potential region), when trimethyl phosphite is added to a solution of II immediately prior to cyclic voltammetry.

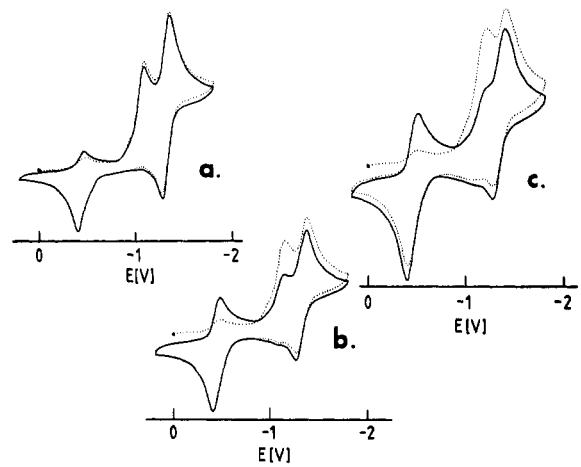

Figure 6. Cyclic voltammetric study of the reduction of the saturated cluster II in THF under a CO atmosphere and containing 0.3 M TBAP at 25 °C: (---) initial cathodic single sweep; (—) steady state at repetitive scans at (a) 100, (b) 500, and (c) 1000 mV s^{-1}.

Table IV. ESR Spectra of the Anion Radical I^{-} and the Cation Radical II^{+}•

ESR	$I^{-}\cdot$[a]	$II^{+}\cdot$[b]
$\langle g \rangle$	2.047	2.046
$a(^{31}P)$, G	29.8 ± 0.1[c]	30.0 ± 0.1[c]

[a] From the reduction of I in THF with 1% sodium amalgam at 25 °C. [b] From the oxidation of II in CH_2Cl_2 with $AgBF_4$ under an atmosphere of CO at 25 °C. [c] Peak-to peak line width of 9 G.

The combination of eq 7 and 9 leads overall to the rapid, reversible dissociation of CO from the anion radical of the saturated cluster, i.e., eq 11.

$$\underset{\text{II}^{-}\cdot}{Cp'RhFe_3(CO)_9(PPh)_2^{-}\cdot} \rightleftharpoons \underset{\text{I}^{-}\cdot}{Cp'RhFe_3(CO)_8(PPh)_2^{-}\cdot} + CO \quad (11)$$

This conclusion is confirmed by the comparison of the initial scan and the cyclic voltammograms obtained at steady state at the various sweep rates shown in Figure 6. Thus at an intermediate sweep rate of 100 mV s^{-1}, the CO dissociation in eq 9 is more or less at equilibrium, and the initial and steady-state cyclic voltammograms are comparable. Note also that the anodic peak current for wave F is somewhat less than that coupled to E at −1.3 V, as a result of the partial loss of $I^{-}\cdot$ by CO pickup. However, at the faster scan rate of 1000 mV s^{-1}, the wave C for $I^{-}\cdot$ increases in the steady-state cyclic voltammogram at the expense of the irreversible wave D due to $II^{-}\cdot$. On this time scale, the reversibility in eq 9 is not achieved, and the CV waves C and E for $I^{-}\cdot$ approach the electrochemical behavior shown in Figure 2.

ESR Spectra of the Anion Radical $I^{-}\cdot$ and the Cation Radical II^{+}. The well-behaved one-electron reduction of the unsaturated cluster I to its anion radical $I^{-}\cdot$ and the well-behaved one-electron oxidation of the saturated cluster II to its cation radical II^{+} permit their esr spectra to be examined (Table IV). In these spectral studies, we found chemical methods to be most appropriate for the generation of the ion radicals as follows.

The reduction of the saturated cluster I was carried out in THF solutions with 1% amalgam, i.e., eq 12. The

$$\underset{\text{I}}{Cp'RhFe_3(CO)_8(PPh)_2} + Na(Hg) \rightarrow \underset{\text{I}^{-}\cdot}{Na[Cp'RhFe_3(CO)_8(PPh)_2]} + (Hg) \quad (12)$$

isotropic ESR spectrum of $I^{-}\cdot$ in Figure 7a consists of a

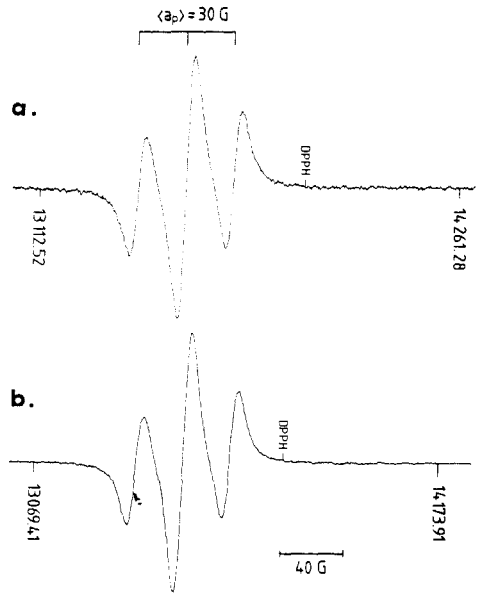

Figure 7. ESR of ion radicals derived from (a) reduction of the unsaturated cluster I with 1% sodium amalgam in THF and (b) oxidation of the saturated cluster II with $AgBF_4$ in methylene chloride both at 25 °C.

1:2:1 triplet at $\langle g \rangle = 2.047$ with $a_P = 29.8$ G due to a pair of equivalent phosphinidene caps.

The saturated cluster II was chemically oxidized in methylene chloride with a solution of silver tetrafluoroborate, to accord with its first oxidation potential in Table III, i.e., eq 13. The isotropic ESR spectrum of $II^{+}\cdot$ in

$$Cp'RhFe_3(CO)_9(PPh)_2 + AgBF_4 \rightarrow \underset{II}{} [Cp'RhFe_3(CO)_9(PPh)_2]BF_4 + Ag \quad (13)$$
$$II^{+}\cdot$$

Figure 7b consists of a 1:2:1 triplet at $\langle g \rangle = 2.046$ with $a_P = 30.0$ G due to a pair of equivalent phosphinidene caps. Whereas the anion radical $I^{-}\cdot$ persists in THF for prolonged periods, the cation radical $II^{+}\cdot$ in methylene chloride slowly decomposes over a period of several hours at room temperature.

Discussion

The rhodium–triiron cluster $(C_5Me_5)RhFe_3(CO)_8(PPh)_2$ (I) represents a closo six-vertex compound which is readily interconverted by CO ligation with another closo six-vertex compound, II. As such, eq 14 is a cluster system similar

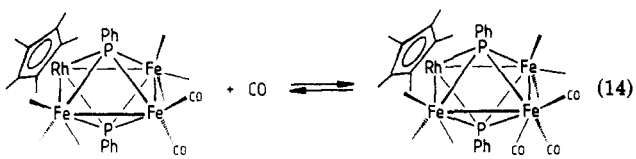

(14)

I. II.

to the bicapped tetrairon carbonyl $Fe_4(CO)_{11}(\mu_4\text{-}PAr)_2$, in which a pair of closo six-vertex structures were shown earlier to be chemically interconvertible.[8] [Note that the skeletal framework of $(C_5Me_5)RhFe_3(CO)_8(PPh)_2$ is isomorphous with that of $Fe_4(CO)_{11}(\mu_4\text{-}PAr)_2$ since $(C_5Me_5)Rh$ and $Fe(CO)_3$ are isolobal fragments.[31]] In both cluster systems, the unsaturated counterpart possesses seven skeletal electron pairs in harmony with Wade's formalism.[19] However the saturated counterparts with eight skeletal electron pairs clearly represent violations of the

(31) Hoffmann, R. *Angew. Chem.* **1982**, *94*, 725.

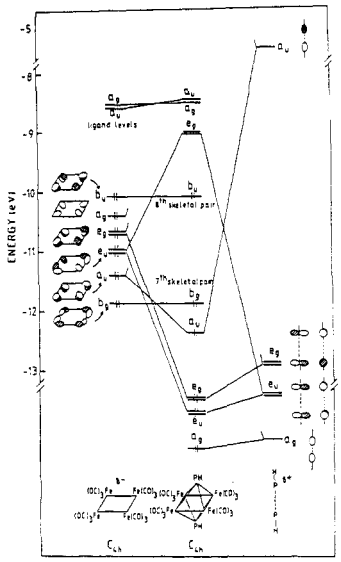

Figure 8. Correlation diagram of the energy levels in the closo six-vertex cluster $M_4(\mu_4\text{-}E)_2$, as represented by $Fe_4(CO)_{12}(PH)_2$ and reproduced from Halet, Hoffman, and Saillard.[15]

rules since the X-ray crystallographic analyses establish in each case the formation of a closo and not a nido structure (in the latter).

A theoretical explanation of this ambiguity was recently presented by Halet, Hoffmann, and Saillard (HHS).[15] For convenience, their molecular orbital interaction diagram for $Fe_4(CO)_{12}(\mu_4\text{-}PH)_2$ is reproduced in Figure 8.[32] According to HHS, the energy gap between the HOMO (b_u) and the subjacent SHOMO (b_g) is modulated by an interaction of the d orbitals on the phosphorus bridge with the set of π-metal orbitals. Depending on the magnitude of this energy gap, it is possible to obtain a stable closo six-vertex cluster with eight or seven skeletal electron pairs.

It follows from the HHS formulation that an equivalent interconversion between unsaturated and saturated clusters can be carried out by electron transfer. Indeed this prediction is nicely borne out by the electrochemical redox studies of clusters I and II shown in Figures 2 and 3. Thus the unsaturated cluster I undergoes a two-electron reduction to the dianion I^{2-} at −1.32 V via a pair of reversible one-electron accessions. Analogously, the saturated cluster II undergoes a two-electron oxidation at +0.96 V to the dication II^{2+} via a pair of reversible one-electron ionizations. The dianion I^{2-} is isoelectronic with the saturated cluster II, and the dication II^{2+} is similarly isoelectronic with the unsaturated cluster I. That these redox changes occur with minimal structural changes is shown by the ESR spectra of the anion radical $I^{-}\cdot$ and the cation radical $II^{+}\cdot$ in Figure 7 representing the semireduction and semioxidation of the unsaturated and saturated clusters, respectively. As such, $I^{-}\cdot$ and $II^{+}\cdot$ represent the same state (b_u in Figure 8), with identical $\langle g \rangle$ values and ^{31}P hyperfine splittings in Table IV. The rather sizeable magnitude of $a_P = 30$ G is consistent with the HHS picture of electron delocalization beyond the planar metal array and onto the phosphinidene bridges.

The addition of another electron to the saturated cluster II populates the rather high-lying LUMO (see e_g in Figure 8). In accord with this formulation, we find the CV wave D at the rather negative potential $E_p^c = -1.1$ V (Figure 3) to be chemically irreversible even at high sweep rates, indicative of the short lifetime (<ms) of the anion radical

(32) We thank Dr. R. Hoffmann for permission to reproduce Figure 8 from ref 15.

$II^{-}\cdot$. The concomitant formation of the anion radical I^{-} of the unsaturated triiron cluster is detected by the appearance on the return scan of the anodic wave F which corresponds to its oxidation to the unsaturated cluster I. Such a transformation represents the dissociative loss of a CO ligand from the metastable $II^{-}\cdot$, i.e., eq 15.

$$\underset{II^{-}\cdot}{Cp'RhFe(CO)_9(PPh)_2^{-}\cdot} \overset{fast}{\rightleftharpoons} \underset{I^{-}\cdot}{Cp'RhFe(CO)_8(PPh)_2^{-}\cdot} + CO \quad (15)$$

The same CV behavior has been observed during the reduction of the coordinatively saturated, 18-electron $Mn(CO)_3(NCMe)_3^{+}$.[30] Furthermore, the modulation of the anodic peak current for the CV wave F by the CV sweep rate as shown in Figure 4 indicates that the loss of CO is reversible. Whereas the equilibrium in eq 15 strongly favors the coordinatively unsaturated anion radical $I^{-}\cdot$, the corresponding equilibrium in eq 14 for ($I \rightleftharpoons II + CO$) does not so strongly differentiate between the neutral precursors. To make further distinctions, the anion radicals in eq 15 appear to interconvert at faster rates than their neutral precursors in eq 14, under more or less comparable conditions.

Experimental Section

Materials. Trimethyl phosphite (Victor Chemical) and triethylphosphine (M and T Chemical) were distilled from sodium and stored under an argon atmosphere. Iron pentacarbonyl and phenyldichlorophosphine (Strem Chemical) were used as received. The triiron cluster $Fe_3(CO)_9(PPh)_2$ was prepared from iron pentacarbonyl and $PhPCl_2$ by the procedure described by Muetterties et al.:[33] mp 132–133 °C; $^{31}P\{^1H\}$ NMR ($CDCl_3$) δ 317 (s); IR (hexane) ν(CO) 2044 (s), 2023 (s), 2008 (s), 1996 (m), 1986 (w) cm^{-1}. The dimeric rhodium(III) chloride $[C_5(CH_3)_5RhCl_2]_2$ was prepared by the procedure described by Kang and Maitlis.[34] Tetra-*n*-butylammonium perchlorate (G. F. Smith Chemical) was recrystallized from a mixture of hexane and ethyl acetate and dried in vacuo prior to use. Silica gel (60–200 mesh) from J. T. Baker was used for column chromatography.

All manipulations were carried out under argon with the aid of standard Schlenk line techniques. Solvents were purified by standard procedures.[35] Melting points are not corrected. Elemental analyses were performed by Atlantic Microlab, Inc., Atlanta, GA.

Instrumentation. The ^1H (89.55-MHz) and ^{31}P (36.23-MHz) NMR spectra were recorded on a JEOL FX-90Q spectrometer. Infrared spectra were obtained on a Nicolet DX-10 FT spectrometer. The X-band ESR spectra were recorded on a Varian Century-line E112 spectrometer equipped with a NMR gaussmeter for field frequency calibration. Cyclic voltammetry was performed at a platinum electrode with an IR-compensated potentiostat[36] driven by a Princeton Applied Research Model 175 universal programmer. Cyclic voltammograms were recorded on a Houston Series 2000 x-y recorder. The $E_{1/2}$ and E_p values were determined by cyclic voltammetry and referred to SCE. The reference electrode was in contact with the solution by a cracked glass tip. The bulk electrolysis cell was of air-tight design with high vacuum teflon valves (Kontes) and viton o-ring seals to allow an inert atmosphere to be maintained on the solution without contamination by grease.

Synthesis of $(C_5Me_5)RhFe_3(CO)_8(PPh)_2$ (I). The triiron cluster $Fe_3(CO)_9(PPh)_2$ (200 mg, 314 mmol) was dissolved in 30 mL of THF and cooled to −78 °C. A 4.2-mL aliquot of a solution of 0.15 M sodium naphthalene in THF was added dropwise; followed by 97 mg (157 mmol) of $[(C_5Me_5)RhCl_2]_2$.[34] The resulting solution was allowed to warm to room temperature and stirred for an additional hour. The brown solution was evaporated to dryness and extracted with hexane to remove $Fe_3(CO)_9(PPh)_2$ and unidentified rhodium compounds. The resulting solid was extracted with benzene to afford a dark brown solution. Chromatography on a short column (3 × 10 cm) of silica gel was followed by concentration of the eluent. Addition of hexane and crystallization at −30 °C yielded 41 mg (48 μmol) of black crystals of I: yield 15%; mp 224 °C; IR (ν(CO), toluene) 2028 (s), 1987 (vs), 1954 (m), 1940 (w) cm^{-1}; ^1H NMR ($CDCl_3$) δ 7.3–6.6 (7, PPh), 2.25 (t, C_5Me_5) $^3J_{PH}$ = 1.7 Hz); ^{31}P NMR (toluene-d_8) δ 227.6 (d, J_{RhP} = 97 Hz). Anal. Calcd for $C_{30}H_{25}Fe_3O_8P_2Rh$ (845.9): C, 42.60; H, 2.98. Found: C, 42.73; H, 2.99.

Synthesis of $(C_5Me_5)RhFe_3(CO)_9(PPh)_2$ (II). The unsaturated cluster $(C_5Me_5)RhFe_3(CO)_8(PPh)_2$ (30 mg, 36 μmol) was dissolved in 5 mL of toluene and the solution stirred for 2 h under an atmosphere of carbon monoxide. The pickup of CO was accompanied by a change in color of the solution from brown to red. Adition of 10 mL of hexane and crystallization at −30 °C yielded 28 mg (32 μmol) of red-black crystals of II: yield 89%; mp 244 °C dec; IR (ν(CO), toluene) 2045 (s), 2008 (vs), 1994 (m), 1977 (s), 1952 (m), 1945 (m) cm^{-1}; ^1H NMR ($CDCl_3$) δ 8.0–7.4 (m, PPh); 1.78 (t, C_5Me_5, J_{PH} = 1.5 Hz); ^{31}P NMR ($CDCl_3$) δ 319.6 (d, J_{RhP} = 82 Hz).

X-ray Crystallography of the Rhodium–Triiron Clusters I and II. Black crystals of I suitable for X-ray diffraction measurements were grown from a hexane solution at −20 °C under an argon atmosphere. Red-black crystals of II were grown from a mixture of toluene and hexane by slow solvent diffusion at 25 °C under a carbon monoxide atmosphere. The crystals were mounted on glass fibers in random orientations and placed on an Enraf-Nonius CAD-4 automatic diffractometer. The crystal data and data collection parameters at 18 °C are listed in Table V. The Mo Kα radiation was monochromatized by a dense graphite crystal assumed for all purposes to be 50% imperfect. The Laue symmetries were determined to be $2/m$, and the space group was shown to be $P2_1/c$ for I and either $P2_1$ or $P2_1/m$ for II. Lorentz and polarization factors were applied in the data reduction, and an empirical absorption correction was based on azimuthal ψ scans of six reflections having χ near 90°.[37]

The structure of I was solved by the Patterson method which revealed the position of the Rh atom. The coordinates of the remaining non-hydrogen atoms in the molecule were found in subsequent difference Fourier syntheses. The usual sequence of isotropic and antisotropic refinement was followed, after which all phenyl hydrogens were entered in ideally calculated positions. The methyl hydrogens were located in difference maps and al-

Table V. Data Collection and Processing Parameters for the Rhodium–Triiron Clusters I and II

	I	II
space group	$P2_1/c$ (monoclinic)	$P2_1$ (monoclinic)
cell constants	16.367 (3)	9.260 (1)
a, Å	10.684 (3)	18.307 (3)
b, Å	19.648 (5)	19.562 (3)
c, Å	110.37 (1)	90.51 (1)
β, deg	3221	3316
V, Å^3		
mol formula	$RhFe_3P_2O_8C_{30}H_{25}$	$RhFe_3P_2O_9C_{31}H_{25}$
fw	845.9	873.9
formula units per cell (Z)	4	4
density (ρ), g·cm^{-3}	1.74	1.75
abs coeff (μ)	19.66	19.1
radiation (λ, Mo Kα), Å	0.710 73	0.710 73
collectn range	$4° \le 2\theta \le 38°$	$4° \le 2\theta \le 46°$
total data collected	2894	5109
independent data, $I > 3\sigma(I)$	2279	4074
total variables	397	608
$R = \sum\|\|F_o\| - \|F_c\|\|/\sum\|F_o\|$	0.018	0.033
$R_w = [\sum w(\|F_o\| - \|F_c\|)^2/\sum w\|F_o\|^2]^{1/2}$	0.021	0.043
weights	$w = \sigma(F)^{-2}$	$w = \sigma(F)^{-2}$

(33) Kouba, J. K.; Muetterties, E. L.; Thompson, M. R.; Day, V. W. *Organometallics* **1983**, *2*, 1609.
(34) Kang, J. W.; Maitlis, P. M. *J. Am. Chem. Soc.* **1968**, *90*, 3259.
(35) Perrin, D. D.; Armarego, W. L.; Perrin, D. R. *Purification of Laboratory Chemicals*; Pergamon: New York, 1980.
(36) Garreau, D.; Saveant, J. M. *J. Electroanal. Chem.* **1972**, *35*, 309; **1974**, *50*, 22.
(37) North, A. C. T.; Phillips, D. C.; Matthews, F. S. *Acta Crystallogr., Sect. A: Cryst. Phys., Diffr., Theor. Gen. Crystallogr.* **1968**, *A24*, 351.

Table VI. Positional Parameters and Their Estimated Standard Deviations in Crystalline $(C_5Me_5)RhFe_4(\mu_4\text{-}PPh)_2(CO)_8$ (I)[a]

atom	x	y	z	B, Å²	atom	x	y	z	B, Å²
Rh	0.760296 (2)	0.23458 (3)	0.38293 (2)	2.440 (8)	C21	0.7805 (3)	0.7409 (4)	0.2792 (2)	5.7 (1)
Fe1	0.85856 (4)	0.34148 (6)	0.51434 (3)	2.89 (1)	C22	0.8517 (3)	0.7208 (5)	0.2602 (2)	5.8 (1)
Fe2	0.73667 (4)	0.49639 (6)	0.50553 (3)	3.36 (2)	C23	0.9038 (3)	0.6209 (5)	0.2876 (2)	5.9 (1)
Fe3	0.63614 (3)	0.40691 (6)	0.38846 (3)	2.90 (1)	C24	0.8847 (3)	0.5377 (5)	0.3339 (2)	4.5 (1)
P1	0.78051 (7)	0.4423 (1)	0.40723 (5)	2.84 (3)	C25	0.6692 (2)	0.1699 (4)	0.5244 (2)	2.9 (1)
P2	0.71740 (7)	0.2782 (1)	0.47858 (5)	2.72 (3)	C26	0.5938 (2)	0.2021 (4)	0.5366 (2)	3.4 (1)
O1	0.9243 (2)	0.1372 (3)	0.6166 (2)	7.3 (1)	C27	0.5553 (3)	0.1190 (4)	0.5694 (2)	4.6 (1)
O2	1.0256 (2)	0.3488 (3)	0.4912 (2)	5.67 (9)	C28	0.5917 (3)	0.0051 (4)	0.5894 (2)	5.7 (1)
O3	0.9070 (2)	0.5142 (3)	0.6368 (2)	6.2 (1)	C29	0.6671 (3)	−0.0294 (4)	0.5791 (2)	5.5 (1)
O4	0.6827 (2)	0.5222 (3)	0.6298 (2)	6.9 (1)	C30	0.7065 (3)	0.0542 (4)	0.5465 (2)	4.0 (1)
O5	0.7852 (2)	0.7588 (3)	0.5204 (2)	7.4 (1)	H14A	0.595 (2)	0.077 (4)	0.197 (2)	6*
O6	0.5597 (2)	0.6168 (3)	0.4381 (2)	7.4 (1)	H14B	0.561 (2)	0.133 (4)	0.253 (2)	6*
O7	0.4720 (2)	0.2724 (4)	0.3529 (2)	7.5 (1)	H14C	0.602 (3)	0.215 (4)	0.207 (2)	6*
O8	0.5744 (2)	0.4952 (4)	0.2399 (2)	7.1 (1)	H15A	0.611 (2)	0.000 (4)	0.363 (2)	6*
C1	0.8970 (3)	0.2164 (4)	0.5758 (2)	4.2 (1)	H15B	0.641 (2)	−0.104 (4)	0.325 (2)	6*
C2	0.9606 (3)	0.3491 (4)	0.5004 (2)	3.8 (1)	H15C	0.679 (3)	−0.079 (4)	0.404 (2)	6*
C3	0.8714 (3)	0.4614 (4)	0.5832 (2)	4.1 (1)	H16A	0.837 (3)	−0.064 (4)	0.465 (2)	6*
C4	0.7029 (3)	0.5095 (4)	0.5806 (2)	4.0 (1)	H16B	0.873 (2)	−0.110 (4)	0.403 (2)	6*
C5	0.7659 (3)	0.6547 (4)	0.5140 (2)	4.3 (1)	H16C	0.904 (2)	0.002 (4)	0.454 (2)	6*
C6	0.6079 (3)	0.5389 (4)	0.4346 (2)	4.2 (1)	H17A	0.968 (2)	0.149 (4)	0.388 (2)	6*
C7	0.5370 (3)	0.3232 (4)	0.3683 (2)	4.2 (1)	H17B	0.949 (2)	0.094 (4)	0.310 (2)	6*
C8	0.5997 (3)	0.4620 (4)	0.2991 (2)	4.1 (1)	H17C	0.941 (3)	0.226 (4)	0.317 (2)	6*
C9	0.6923 (2)	0.1327 (4)	0.2824 (2)	2.9 (1)	H18A	0.771 (3)	0.226 (4)	0.181 (2)	6*
C10	0.7177 (2)	0.0463 (4)	0.3410 (2)	2.9 (1)	H18B	0.810 (3)	0.323 (4)	0.236 (2)	6*
C11	0.8104 (2)	0.0485 (4)	0.3719 (2)	3.0 (1)	H18C	0.726 (3)	0.320 (4)	0.197 (2)	6*
C12	0.8414 (2)	0.1352 (4)	0.3313 (2)	3.2 (1)	H20	0.7111	0.6730	0.3376	5*
C13	0.7685 (2)	0.1870 (4)	0.2759 (2)	3.1 (1)	H21	0.7447	0.8117	0.2609	5*
C14	0.6009 (3)	0.1518 (4)	0.2310 (2)	4.6 (1)	H22	0.8645	0.7762	0.2273	5*
C15	0.6575 (3)	−0.0383 (4)	0.3615 (2)	4.5 (1)	H23	0.9549	0.6066	0.2748	5*
C16	0.8663 (3)	−0.0356 (5)	0.4306 (2)	5.0 (1)	H24	0.9221	0.4672	0.3531	5*
C17	0.9362 (3)	0.1540 (5)	0.3410 (2)	5.1 (1)	H26	0.5674	0.2812	0.5217	5*
C18	0.7715 (3)	0.2751 (5)	0.2185 (2)	5.1 (1)	H27	0.5035	0.1409	0.5781	5*
C19	0.8130 (2)	0.5560 (4)	0.3528 (2)	3.2 (1)	H28	0.5644	−0.0527	0.6117	5*
C20	0.7609 (3)	0.6588 (4)	0.3249 (2)	4.8 (1)	H29	0.6910	−0.1098	0.5931	5*
					H30	0.7597	0.0320	0.5395	5*

[a] Anisotropically refined atoms are given in the form of the isotropic equivalent thermal parameter defined as $(^4/_3)[a^2B(1,1) + b^2B(2,2) + c^2B(3,3) + ab(\cos\gamma)\,B(1,2) + ac(\cos\beta)B(1,3) + bc(\cos\alpha)B(2,3)]$. Asterisk identifies atoms refined isotropically.

lowed to refine independently until the final cycles of the least squares.

The structure of II was solved by Multan[38] which revealed the positions of all eight metal atoms present as two independent molecules which comprise the asymmetric unit. The space group $P2_1$ was assumed to be correct on the basis of the statistical analysis of the unitary structure factors, which gave near perfect agreement with theoretical values. Owing to the larger numbers of non-hydrogen atoms, only the core atoms and carbonyl ligands were refined anisotropically, with the phenyl and cyclopentadienyl carbon atoms being treated isotropically. No effort was made to locate or ideally position any of the hydrogen atoms. As can be seen from the packing diagram in Figure 9, there are no *m* or $\bar{1}$ symmetry elements between the independent molecules, thus confirming $P2_1$. Since the β angle was close to 90°, a careful check was made to preclude the possibility of Laue symmetry mmm. The refinement of the inverted structure yields a *R* value insignificantly different from the present refinement. Thus no further attempt was made to determine the absolute configuration. Graphic analysis of the two independent molecules shows them to be virtually superimposable. All calculations were made by using the Molecular Structure Corp.'s TEXRAY 230 modification of the SDP-PLUS series of programs. Final fractional coordinates with esd's are given for I in Table VI and for the two independent molecules a and b of II in Table VII.

Description of the Molecular Structures of the Rhodium–Triiron Clusters I and II. The four metal atoms in the unsaturated rhodium–triiron cluster I describe a slightly distorted planar rectangle with a pair of longer (Rh–Fe) and a pair of shorter (Fe–Fe) edges. The angle FeRhFe (83.4°) is the smallest, and the angle FeFeFe (93.6°) is the largest. The bridging of each face of the rectangle by a pair of μ_4-phosphinidene caps completes the octahedral core of the cluster. Whereas the Rh–Fe distances of

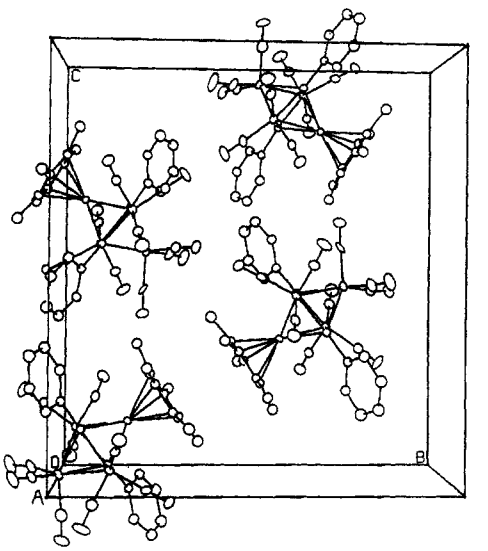

Figure 9. Packing diagram of the unit cell in crystalline $(C_5Me_5)RhFe_3(PPh)_2(CO)_9$ (II).

2.77 Å are in the normal range,[39] the Fe–Fe bonds of 2.55 and 2.51 Å are significantly shorter than those found in such related systems as $Fe_3(\mu_3\text{-}PPh)_2(CO)_9$ (2.71 Å)[40] or the nonbridged metal–metal distances in $Fe_4(\mu_4\text{-}PPh)_2(CO)_{11}$ (2.69 Å)[8] but longer than the carbonyl-bridged, Fe–Fe bond (2.44 Å) in the latter. The intermediate values of the bond distances in I are associated with the semibridging carbonyl ligands[41] that are attached to the iron

(38) Germain, G.; Main, P.; Woolfson, M. M. *Acta Crystallogr., Sect. A: Cryst. Phys., Diffr. Theor. Gen. Crystallogr.* **1971**, *A27*, 368.

(39) For example, consider the average of d_{Rh-Rh} (2.84 Å) in $Rh_4(\mu_4\text{-}PPh)_2(COD)_4$[25] and d_{Fe-Fe} (2.70 Å) in $Fe_4(\mu_4\text{-}P(p\text{-}CH_3C_6H_4))_2(CO)_{11}$.[4,8,23]

(40) Cook, S. L.; Evans, J.; Gray, L. R.; Webster, M. *J. Organomet. Chem.* **1982**, *236*, 367.

Table VII. Positional Parameters and Their Estimated Standard Deviations in Crystalline $(C_5Me_5)RhFe_3(\mu_4\text{-}PPh)_2(CO)_9$ (II)[a]

atom	x	y	z	B, Å²	atom	x	y	z	B, Å²
		Molecule a					Molecule b		
Rh	0.85477 (9)	0.188	0.15987 (4)	1.91 (2)	Rh′	0.62197 (9)	0.56420 (6)	0.33863 (4)	1.92 (2)
Fe1	0.7122 (2)	0.0575 (1)	0.13747 (9)	2.43 (3)	Fe1′	0.4717 (2)	0.6899 (1)	0.36358 (8)	2.42 (3)
Fe2	0.9046 (2)	0.0241 (1)	0.04239 (9)	2.69 (4)	Fe2′	0.6619 (2)	0.7226 (1)	0.46155 (9)	2.67 (4)
Fe3	1.0431 (2)	0.1496 (1)	0.06163 (8)	2.21 (3)	Fe3′	0.8056 (2)	0.5986 (1)	0.44095 (8)	2.20 (3)
P1	0.9584 (3)	0.0768 (2)	0.1472 (2)	2.10 (6)	P1′	0.7203 (3)	0.6777 (2)	0.3565 (2)	2.19 (6)
P2	0.7970 (3)	0.1391 (2)	0.0563 (2)	2.17 (6)	P2′	0.5595 (3)	0.6097 (2)	0.4430 (2)	2.15 (6)
O1	0.729 (1)	−0.0725 (6)	0.2219 (6)	6.1 (3)	O1′	0.486 (1)	0.8244 (5)	0.2799 (5)	5.4 (2)
O2	0.450 (1)	0.0318 (7)	0.0549 (5)	6.1 (3)	O2′	0.211 (1)	0.7187 (7)	0.4475 (5)	5.7 (3)
O3	0.5316 (9)	0.1194 (6)	0.2454 (5)	4.7 (2)	O3′	0.2941 (9)	0.6312 (6)	0.2554 (5)	4.4 (2)
O4	1.155 (1)	−0.0709 (6)	0.0496 (6)	6.0 (3)	O4′	0.910 (1)	0.8217 (6)	0.4750 (6)	6.5 (3)
O5	0.857 (1)	0.0305 (7)	−0.1076 (5)	6.7 (3)	O5′	0.607 (1)	0.7163 (6)	0.6097 (5)	5.7 (3)
O6	1.3035 (8)	0.1779 (6)	0.1436 (5)	4.7 (2)	O6′	1.0652 (8)	0.5817 (6)	0.3575 (5)	4.2 (2)
O7	1.022 (1)	0.2912 (5)	−0.0101 (5)	4.5 (2)	O7′	0.794 (1)	0.4574 (5)	0.5084 (5)	4.4 (2)
O8	1.212 (1)	0.0901 (7)	−0.0494 (5)	6.2 (3)	O8′	0.965 (1)	0.6584 (7)	0.5570 (5)	6.0 (3)
O31	0.715 (1)	−0.1034 (6)	0.0495 (7)	8.5 (3)	O31′	0.474 (1)	0.8528 (5)	0.4499 (5)	5.3 (3)
C1	0.726 (1)	−0.0224 (7)	0.1906 (7)	3.3 (3)	C1′	0.484 (1)	0.7732 (7)	0.3125 (7)	3.0 (3)
C2	0.549 (1)	0.0444 (8)	0.0859 (7)	3.7 (3)	C2′	0.315 (1)	0.7060 (8)	0.4151 (7)	3.6 (3)
C3	0.613 (1)	0.1019 (7)	0.2028 (7)	3.3 (3)	C3′	0.373 (1)	0.6497 (7)	0.2981 (6)	3.3 (3)
C4	1.058 (1)	−0.0323 (7)	0.0478 (7)	3.4 (3)	C4′	0.813 (1)	0.7840 (8)	0.4661 (8)	4.4 (3)
C5	0.873 (1)	0.0300 (9)	−0.0501 (8)	4.3 (3)	C5′	0.625 (1)	0.7164 (7)	0.5517 (7)	3.7 (3)
C6	1.199 (1)	0.1669 (7)	0.1123 (6)	2.9 (3)	C6′	0.965 (1)	0.5898 (7)	0.3888 (6)	3.2 (3)
C7	1.028 (1)	0.2363 (7)	0.0170 (6)	3.0 (3)	C7′	0.794 (1)	0.5130 (7)	0.4827 (6)	2.6 (3)
C8	1.140 (1)	0.1117 (8)	−0.0052 (7)	3.8 (3)	C8′	0.900 (1)	0.6373 (8)	0.5107 (6)	3.3 (3)
C9	0.811 (1)	0.2414 (7)	0.2631 (6)	2.6 (2)*	C9′	0.582 (1)	0.5171 (7)	0.2330 (6)	2.7 (2)*
C10	0.960 (1)	0.2547 (7)	0.2457 (6)	2.6 (2)*	C10′	0.730 (1)	0.5040 (7)	0.2508 (6)	2.2 (2)*
C11	0.956 (1)	0.2980 (7)	0.1837 (6)	2.7 (2)*	C11′	0.733 (1)	0.4605 (7)	0.3117 (6)	2.7 (2)*
C12	0.807 (1)	0.3109 (7)	0.1659 (6)	2.8 (2)*	C12′	0.584 (1)	0.4439 (7)	0.3301 (6)	2.6 (2)*
C13	0.718 (1)	0.2753 (7)	0.2137 (6)	2.7 (2)*	C13′	0.492 (1)	0.4775 (7)	0.2825 (6)	2.7 (2)*
C14	0.769 (1)	0.2075 (7)	0.3298 (6)	3.3 (3)*	C14′	0.528 (1)	0.6619 (8)	0.1687 (7)	3.7 (3)*
C15	1.089 (1)	0.2367 (8)	0.2858 (7)	3.5 (3)*	C15′	0.861 (1)	0.5288 (7)	0.2119 (6)	3.2 (3)*
C16	1.082 (1)	0.3369 (8)	0.1545 (7)	4.0 (3)*	C16′	0.862 (1)	0.4238 (8)	0.3399 (7)	3.5 (3)*
C17	0.751 (1)	0.3593 (8)	0.1075 (7)	4.2 (3)*	C17′	0.532 (1)	0.3931 (9)	0.3859 (7)	4.2 (3)*
C18	0.555 (1)	0.2844 (8)	0.2185 (7)	3.8 (3)*	C18′	0.334 (1)	0.4649 (8)	0.2755 (7)	4.1 (3)*
C19	1.067 (1)	0.0351 (7)	0.2124 (6)	2.4 (2)*	C19′	0.827 (1)	0.7247 (7)	0.2926 (6)	2.8 (2)*
C20	1.023 (1)	0.0309 (8)	0.2787 (7)	3.5 (3)*	C20′	0.781 (1)	0.7225 (7)	0.2253 (6)	3.1 (3)*
C21	1.098 (1)	−0.0030 (8)	0.3295 (7)	3.7 (3)*	C21′	0.862 (2)	0.7561 (9)	0.1748 (8)	4.7 (3)*
C22	1.234 (1)	−0.0314 (8)	0.3150 (8)	4.3 (3)*	C22′	0.993 (2)	0.7910 (9)	0.1922 (8)	4.4 (3)*
C23	1.289 (1)	−0.0267 (8)	0.2495 (7)	3.4 (3)*	C23′	1.042 (2)	0.7927 (9)	0.2575 (7)	4.4 (3)*
C24	1.205 (1)	0.0061 (7)	0.1977 (7)	3.1 (3)*	C24′	0.960 (1)	0.7674 (8)	0.3096 (7)	3.9 (3)*
C25	0.682 (1)	0.1880 (7)	−0.0056 (5)	2.1 (2)*	C25′	0.445 (1)	0.5614 (7)	0.5021 (6)	2.5 (2)*
C26	0.732 (1)	0.2026 (8)	−0.0711 (7)	3.5 (3)*	C26′	0.491 (1)	0.5478 (7)	0.5696 (6)	2.9 (2)*
C27	0.643 (1)	0.2452 (8)	−0.1150 (7)	4.0 (3)*	C27′	0.395 (1)	0.5075 (8)	0.6120 (7)	3.6 (3)*
C28	0.514 (2)	0.2692 (9)	−0.0949 (8)	4.5 (3)*	C28′	0.267 (2)	0.4825 (9)	0.5899 (8)	4.6 (3)*
C29	0.462 (2)	0.2530 (9)	−0.0269 (7)	4.5 (3)*	C29′	0.220 (1)	0.4950 (8)	0.5195 (7)	4.0 (3)*
C30	0.550 (1)	0.2133 (7)	0.0170 (6)	3.1 (3)*	C30′	0.310 (1)	0.5344 (8)	0.4759 (7)	3.3 (3)*
C31	0.785 (2)	−0.0485 (8)	0.0511 (8)	5.2 (4)	C31′	0.541 (1)	0.8005 (8)	0.4508 (7)	3.6 (3)

[a] Anisotropically refined atoms are given in the form of the isotropic equivalent thermal parameter defined as $(^4/_3)[a^2B(1,1) + b^2B(2,2) + c^2B(3,3) + ab(\cos\gamma)\,B(1,2) + ac(\cos\beta)B(1,3) + bc(\cos\alpha)B(2,3)]$. Asterisk identifies atom refined isotropically.

atoms bonded to the rhodium atom and inclined toward the coordinatively unsaturated iron atom. The bond distances between the formally saturated metal atoms and the pair of capping phosphorus atoms are essentially the same (2.27–2.31 Å), whereas the Fe–P bonds to the unsaturated iron dicarbonyl fragments are somewhat longer (2.37 Å). The most interesting feature of the ligand sphere is directed to the two semibridging carbonyl groups along the Fe–Fe bonds. By comparison with the geometric data of well-behaved CO bridges found in a variety of other polynuclear iron compounds,[43] the two ligands are best described as unsymmetrical or semibridging.[42] The remaining six carbonyl groups show no such anomaly as terminal ligands. The average Rh–C bond distance of the symmetrically coordinated pentamethylcyclopentadienyl ligand is 2.20 Å. The methyl substituents are bent out of the ring plane by an average of 5.7° away from the cluster core. Finally, the conformation of the phenyl rings attached to the phosphidene caps orients them parallel to each other, with the planes bisecting one Fe–Fe and one Rh–Fe bond. The strucure of the unsaturated cluster I described in this way compares with the two earlier examples of this type of cluster with 66 skeletal electrons, viz., $Fe_4(\mu_4\text{-}PPh)_2(CO)_{11}$[4,8,23] and $Ru_4(\mu_4\text{-}PPh)_2(CO)_{11}$.[44] In the latter, the short metal–metal bond along the coordinatively unsaturated centers of the cluster core is bridged symmetrically by a carbonyl group. By contrast, the unsaturated nature of I is localized at one iron atom making Fe(2) a formally 16-electron center. This electron deficiency could account for the existence of two semibridging CO groups in inherently unsymmetrical environments.[42b] The Ortep perspective in Figure 10 shows the presence of bent carbonyl ligands attached to Fe(1) and Fe(3) leaning toward the unsaturated center at Fe(2) with the distances Fe(2)–C(3) of 2.23 Å and Fe(2)–C(6) of 2.13 Å which very much resemble those of semibridging contacts. The origin of this structural feature, however, cannot be distinguished between two possibilities, namely, (a) the weak Fe···CO interactions as a convenient way of maintaining the electron balance in the solid state[45] or (b) a steric effect of the bulky pentamethylcyclopentadienyl ligand which provides a backside buttress to force these CO groups toward Fe(2). Coordinative unsaturated alone is not sufficient

(41) Both carbonyls are by definition[42] semibridging two-electron ligands.

(42) See, e.g.; (a) Horowitz, C. P.; Shriver, D. F. *Adv. Organomet. Chem.* **1984**, *23*, 219. (b) Cotton, F. A.; Wilkinson, G. *Advanced Inorganic Chemistry* 4th ed.; Wiley: New York, 1980; p 1057 ff.

(43) Colton, R.; McCormick, M. J. *Coord. Chem. Rev.* **1980**, *31*, 1.

(44) Field, J. S.; Haines, R. J.; Smit, D. N. *J. Organomet. Chem.* **1982**, *224*, C49.

(45) Cotton, F. A. *Prog. Inorg. Chem.* **1976**, *21*, 1.

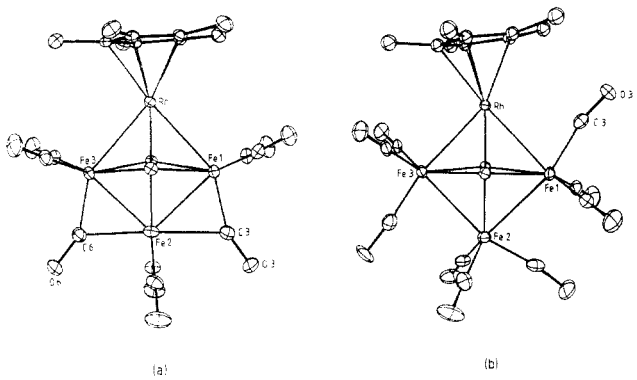

Figure 10. Ortep perspectives from the top of (a) the unsaturated cluster I and (b) the saturated cluster II, as viewed along an axis through the phosphorus atoms, showing the stereochemistry of the carbonyl ligand sphere. The phenyl substituents and hydrogen atoms are omitted for clarity.

to promote the semibridging bonding mode, since the heterotrimetallic cluster $(\eta^5\text{-}C_5H_5)NiFe_2Co(\mu_4\text{-}PPh)_2(CO)_8$, which has two more electrons than **I** and is classified as a saturated cluster with 68 electrons, also shows evidence of possessing semibridging carbonyl groups.[46]

The four metal atoms in the saturated rhodium–triiron cluster II are essentially the same as that described above for the unsaturated cluster I. Accordingly let us concentrate on the structural changes attendant upon the addition of CO ligand to convert a 66-electron unsaturated cluster to a 68-electron saturated one. The increase of the electron count by two not only is reflected in an expansion of the cluster core but also results in significant changes in the ligand sphere. Although the Rh–Fe distances do not vary significantly, the Fe–Fe bonds of 2.66 Å are expanded by 0.11 and 0.15 Å so that the four metal atoms now form a near perfect square. The distances to the fourfold bridging phosphinidene caps do not vary significantly—except that to Fe(2). Here a change from 2.37 to 2.31 Å is remarkable, particularly if one considers the fact that the metal center in II carries one more ligand than that in I. The ligand sphere in I contains nine terminal CO groups, whose orientations are determined by repulsive interactions around the iron centers. In particular, the CO ligand pointing toward the C_5Me_5 group has an Fe(1)–C(3)–O(3) angle of 167° which we interpret as arising from steric compression. This is also reflected in the longer Rh–C bonds (2.27 Å) by 0.07 Å and a larger buckling (average 9.0°) of the methyl substituents relative to the cyclopentadienyl plane away from the cluster core. It can also be seen in Figure 10 that the C_5Me_5 group is tilted toward Fe(3) owing to the steric repulsion of one carbonyl C(3) ligand bound to Fe(1). Despite the electronic differences between I and II, the orientation of the terminal CO ligands in both is dominated by steric effects which minimize the repulsive interactions among the ligands. Thus the "staggered" arrangement of the $Fe(CO)_3$ units in II is readily apparent in Figure 10b. In this sense, even the C_5Me_5 group has an optimized conformation relative to the carbonyl ligands. Finally, the nonbonded distance between the phosphorus caps shrinks from 2.67 Å in I to 2.59 Å in II. This agrees with the general observation that the P–P distances in clusters with seven skeletal electron pairs are longer than those with eight electron pairs,[15] presumably due to the geometric effect arising from the elongation of the metal–metal bonds.

It has been suggested that the elimination of carbon monoxide from the saturated 68-electron cluster $Fe_4(\mu_4\text{-}PPh)_2(CO)_{12}$ is induced by the crowding of ligands.[8] The rhodium–triiron cluster represents a particularly compelling example of this effect, since there is only a minimal structural change of the cluster accompanying CO loss. We indeed believe that steric requirements are necessary to induce CO elimination of the otherwise electronically preferred saturated cluster. Thus the fine tuning of electronic and steric effects are responsible for the particular ease with which the addition-elimination equilibrium of CO ligands is attained in eq 3.

Isotopic ^{13}CO Exchange and the Structures of I and II in Solution. The isotopic exchange of carbonyl ligands was carried out by initially dissolving 30 mg of I in 10 mL of benzene and exposing the solution to an atmosphere of ^{13}C-enriched (99%) carbon monoxide. Within minutes the initially dark brown solution turned red. After 3 days of exposure to ^{13}CO, the flask was evacuated until the solution returned to its original dark brown color (8 h). Evaporation of the solvent yielded ^{13}CO-enriched I as a dark brown-black powder: ^{13}C NMR (toluene-d_8) δ 225.4 and 209.1 with an intensity ratio of 3:1. A sample of this material was dissolved in toluene-d_8 and sealed in a NMR tube under an atmosphere of ^{13}CO. The initially dark brown solution became red, characteristic of II: ^{13}C NMR (toluene-d_8) δ 213.8 and 212.8.

Attempts to detect the semibridging carbonyl ligands in solution were considered in the following manner. The temperature-dependent ^{13}C NMR spectrum of a ^{13}CO-enriched sample of I does not show evidence of the structure determined in the solid state. Thus the sharp singlet resonances at δ 225.4 and 209.1 remained unchanged between −90 and +50 °C. By analogy with the fluxional behavior of $Fe_3(CO)_9(PPh)_2$ established by Muetterties and co-workers,[47] we interpret the temperature-insensitive behavior to a low barrier to site exchange at the $Fe(CO)_3$ centers. Moreover the absence of line broadening also militates against the positional exchanges of CO between iron centers in this temperature range. Similarly, a ^{13}CO-enriched sample of II exhibits two sharp singlet resonances at δ 213.8 and 212.8, which accords with a facile fluxional interchange of CO ligands in $Fe(CO)_3$ units on the NMR timescale but no intermetal ligand exchange.

Cyclic Voltammetry. The oxidation reduction behavior of the unsaturated cluster I, was determined by cyclic voltammetry of 1×10^{-3} M THF solutions containing 0.3 M TBAP under an argon atmosphere. The saturated cluster II was examined under similar conditions, except a CO atmosphere was maintained over the solution.

ESR Spectra. A solution of the unsaturated cluster I in THF was reduced to $I^{-}\cdot$ with 1% sodium amalgam at 25 °C directly in an ESR tube under argon. The tube was sealed and the ESR spectrum measured, as described previously.[48] The ESR spectrum of the cation radical $II^{+}\cdot$ of the saturated cluster was obtained in methylene chloride by the oxidation of II with $AgBF_4$ under a CO atmosphere. The line width of 9 G in the ESR spectra of both $I^{-}\cdot$ and $II^{+}\cdot$ precluded more accurate values of the esr parameters than those listed in Table IV.

Acknowledgment. We thank Dr. J. D. Korp for the crystal structures of I and II and the National Science Foundation and the Robert A. Welch Foundation for financial support. H.H.O. is a recipient of a NATO grant administered under the auspices of the German Academic Exchange Service.

Registry No. I, 101858-53-1; I^{-}, 101858-52-0; II, 101834-97-3; II^{+}, 101834-98-4; $Fe_3(CO)_9(PPh)_2$, 38903-71-8; $[(C_5Me_5)RhCl_2]_2$, 12354-85-7.

Supplementary Material Available: Tables of complete bond distances, bond angles, anisotropic thermal parameters, and structure factor amplitudes for the rhodium–triiron clusters I and II (46 pages). Ordering information is given on any current masthead page.

(46) Müller, M.; Vahrenkamp, H. *Chem. Ber.* **1983**, *116*, 2765.

(47) Kouba, J. K.; Muetterties, E. L., Thompson, M. R.; Day, V. W. *Organometallics* **1983**, *2*, 1065.

(48) Lau, W.; Huffman, J. C.; Kochi, J. K. *Organometallics* **1982**, *1*, 155.